OPEN ACCESS

University of BRISTOL

Zhou, W., & Yuan, X. (2020). Experimental Evaluation of SiC MOSFETs in Comparison to Si IGBTs in a Soft-switching Converter. *IEEE Transactions on Industry Applications*. https://doi.org/10.1109/TIA.2020.2999440

Publisher's PDF, also known as Version of record

Link to published version (if available):
10.1109/TIA.2020.2999440

Link to publication record in Explore Bristol Research
PDF-document

This is the author accepted manuscript (AAM). The final published version (version of record) is available online via Institute of Electrical and Electronics Engineers at https://ieeexplore.ieee.org/document/9106748 . Please refer to any applicable terms of use of the publisher.

University of Bristol - Explore Bristol Research
General rights

This document is made available in accordance with publisher policies. Please cite only the published version using the reference above. Full terms of use are available:
http://www.bristol.ac.uk/red/research-policy/pure/user-guides/ebr-terms/

Experimental Evaluation of SiC MOSFETs in Comparison to Si IGBTs in a Soft-switching Converter

Wenzhi Zhou, *Student Member, IEEE*, Xibo Yuan, *Senior Member, IEEE*

***Abstract*—SiC MOSFETs have shown superior characteristics to Si IGBTs, bringing in significant performance improvement such as enabling more compact, higher efficiency converters that are not feasible with conventional Si IGBTs. Currently, there is a lack of systematic and conclusive investigation into soft-switching inverters using SiC MOSFETs in comparison to Si IGBTs. This paper, therefore, presents a comparative evaluation of a soft-switching inverter, i.e. the auxiliary resonant commutated pole inverter (ARCPI) using SiC MOSFETs or Si IGBTs. The switching transition, switching device current stress, neutral point ripple current, electromagnetic interference (EMI), efficiency and cost are compared on identical ARCPI setups, i.e. with the same PCBs and under identical driving conditions (gate drivers). Experimental results show that the ARCPI using SiC MOSFETs has better performance than that using Si IGBTs due to its faster switching speed. Firstly, the ARCPI using SiC MOSFETs performs full zero-voltage switching and the switching transition behaviour is more predictable. Unlike Si IGBTs, SiC MOSFETs have no turn-off tail current and forward voltage drop during switching transitions. Secondly, the ARCPI using SiC MOSFETs endures less current stress and smaller ripple current in dc-link capacitors. Thirdly, the ARCPI using SiC MOSFETs exhibits better EMI performance and higher efficiency. Specifically, a maximum 20 dBμV harmonic reduction can be achieved around 800 kHz and a 3.1% improvement in efficiency can be achieved at 6 kW.**

Index Terms — Auxiliary Resonant Commutated Pole Inverter, Efficiency, Si IGBT, SiC MOSFET, Soft-switching.

I. Introduction

THE technical maturity and the commercial availability of wide-bandgap (WBG) power semiconductor devices such as silicon-carbide (SiC) MOSFETs are enabling rapid and transformative advances in power electronics because of their superior characteristics [1-4]. Compared with silicon (Si) power switching devices, SiC devices can work at faster switching speeds, higher operating temperatures and higher voltages [5-7]. The enhancement in the switching speed can reduce the switching loss, thus achieving high efficiency or higher switching frequency [8, 9]. With higher switching frequency, the converter power density can be improved because of the reduction of passive components such as dc-link capacitors and bulky filter inductors [10-12]. The high temperature capability will further improve the power density due to the reduced cooling requirement [13]. The high voltage rating of SiC MOSFETs, e.g. 10kV+ provides an alternative choice for medium voltage applications [1, 2]. Due to the enumerated advantages above, SiC MOSFETs have the potential to replace Si IGBTs in various applications. SiC MOSFETs are being adopted in existing and emerging applications such as transportation and renewable energy systems where higher efficiency and higher power density are demanded [1].

While SiC MOSFETs bring in clear opportunities to enhance operating frequency, efficiency and power density, the ultra-fast switching speed causes several undesirable side-effects, posing challenges in the application of SiC MOSFETs [13-17]. For example, converters using SiC MOSFETs are more susceptible to parasitic elements including circuit parasitic inductance/capacitance from PCB traces, power device itself and packaging, as well as load, causing excessive overshoots and ringings during switching transitions [14-16]. This would degrade the converter efficiency and increase device stress. Besides, high dv/dt of SiC MOSFETs can intensify crosstalk effects, producing spurious turn-on gate voltage or negative turn-off gate voltage in phase leg arrangements [14], which may cause short-circuit or device gate failure. Another issue is the electromagnetic interference (EMI) caused by the high dv/dt, and high switching frequency [17]. The high dv/dt will also cause issues on loads such as motor insulation and bearing degradation. However, it is difficult to deal with the side effects caused by the fast switching speed of SiC MOSFETs when they work in a standard hard switching configuration.

Several possible solutions such as adding an output inductor [18], alternative topologies [9] or waveform shaping through gate control [19], multilevel [20] and soft-switching techniques [21] can be adopted to mitigate the side-effects caused by the ultra-high switching speed of SiC MOSFETs. Among these methods, soft-switching can mitigate the current/voltage overshoots, cross-talk, EMI as well as converter-load interference while maintaining high efficiency because the output waveforms are smoothed due to resonant operation and the voltage and current of switching devices are decoupled [22]. This paper will mainly focus on the soft-switching converters and a review is given as follows.

Soft-switching inverters were proposed to improve the efficiency of inverters based on Si IGBTs [22-31]. In soft-

This work was supported in part by the UK EPSRC National Centre for Power Electronics under Grant EP/R004137/1. (Corresponding author: Xibo Yuan.)

W. Zhou and X. Yuan are with the Department of Electrical and Electronic Engineering, University of Bristol, Bristol, BS8 1UB, U.K. (email: wenzhi.zhou@bristol.ac.uk; xibo.yuan@bristol.ac.uk).

switching inverters, the switching loss can be reduced or even eliminated as the main switches can perform zero voltage switching (ZVS) or zero current switching (ZCS) [23]. Many papers have investigated soft-switching topologies, modeling, control, optimized design methods, and their applications comprehensively and conclusively [23-30]. While many topologies have been proposed, they can be classified as resonant dc-link inverters (RDCIs) and pole commutated inverters (PCIs) [23]. Compared with RDCIs, PCIs are easier to control and have higher efficiency, so most papers investigate the PCIs [4]. Besides topologies, control and optimized design of soft-switching inverters are also studied to reduce switching loss and improve efficiency [27-30]. For example, [29] introduced a variable-timing control method to improve the efficiency of a PCI by 1.25%. [30] improved the efficiency by employing a new optimized holistic design method. It shows a 30% loss saving when compared to the hard switching counterpart. In addition to improving the efficiency, soft-switching inverters can also be used to attenuate high-frequency EMI because they work in a resonant mode and the output voltage edges are slowed and smoothed. For example, [22] employed a soft-switching inverter to address the EMI at its source. It indicates that the soft-switching inverter can attenuate the output voltage harmonic by 37 dB at 4 MHz compared to hard-switching.

Compared with soft-switching inverters using Si IGBTs, the research on soft-switching inverters using SiC MOSFETs is relatively limited. For example, [31] presents a calorimetric method to measure the soft-switching loss using SiC MOSFET modules. [32] extended the switching frequency of a grid-tied SiC MOSFET based soft-switching inverter to 300 kHz while maintaining high efficiency. [33] employed a soft-switching inverter to address the crosstalk effect caused by the high switching speed of SiC MOSFETs.

While soft-switched SiC MOSFET converters are gaining increasing attention, there is still a lack of systematic and conclusive investigation. There are several questions to be answered: for example, can SiC MOSFETs replace Si IGBTs directly in a soft-switching inverter? If they can, are there other opportunities or specific issues by replacing the Si IGBTs with SiC MOSFETs? Do SiC MOSFETs differ significantly from Si IGBTs in device behavior in a soft-switching inverter? How much efficiency can be improved compared with Si IGBTs? Do the soft-switching inverters using SiC MOSFETs have better or worse EMI performance than that using Si IGBTs?

Comparing the performance of these two types of semiconductors can fully demonstrate the superior characteristics of SiC MOSFETs as well as reveal the challenges in the application of SiC devices. This can facilitate the understanding of the device characteristics and the full exploration of the superior characteristics of SiC MOSFETs while attenuating their side-effects. Therefore, the comparison should be carried out between Si IGBTs and SiC MOSFETs to see what benefits can be gained by replacing Si IGBTs with SiC MOSFETs in soft-switching inverters.

This paper aims to provide a useful reference for researchers and engineers to accelerate the adoption of SiC devices in real applications. This paper is based on our previous conference publication [34], which preliminarily compares the performance of soft-switching inverters using SiC MOSFETs or using Si IGBTs. The auxiliary resonant commutated pole inverter (ARCPI) is chosen for study as it is an exemplar PCI with a relatively simple structure, high degree of PWM compatibility and easy control [22, 23, 34]. To obtain objective results, the ARCPI using Si IGBTs and using SiC MOSFETs are built on the same three-phase, 6 kW platform with identical printed circuit boards (PCBs), gate drives and device packaging. This paper will present and investigate the performance differences such as the switching transition, switching current stress, efficiency and EMI based on experimental results.

Compared with the conference version [34], the new contributions/differences in this work are:

1) The experimental prototype is optimised by using different switching devices in this work. Specially, compared with the prototype in [34], when the output power is 6 kW, the efficiency of using SiC MOSFETs and using Si IGBT improves from 95.1% to 95.4% and from 91.2% to 92.3%, respectively.
2) The switching transients including the turn-on and turn-off processes are investigated comprehensively in this work. In this paper, eight signals including the gate signal, drain-source voltage and source current for the main switches and auxiliary switches are captured simultaneously providing detailed information to analyze the switching transients.
3) Besides the switching transient performance, the current stress of the main switches and auxiliary switches, the resonant interval, the ripple current in the capacitor bank at different load conditions are analyzed and compared in this work.
4) In addition, the size of passive components and the cost of the prototype are compared.

The rest of the paper is structured as follows. Section II briefly describes the ARCPI and its commutation process and the experimental setup. Section III presents the experimental results and discusses the performance difference. Section IV draws the conclusions.

II. The ARCPI and Experimental Setup

A. The ARCPI Topology

Fig. 1 shows a single-phase ARCPI [34], which consists of a main phase-leg S_1/D_1, S_4/D_4, an auxiliary resonant circuit and a protection circuit. The auxiliary resonant circuit consists of two auxiliary switches S_{a1}/D_{a1}, S_{a4}/D_{a4}, a resonant inductor L_r and two snubber capacitors C_{r1}, C_{r4} in parallel with the main switches S_1/D_1, S_4/D_4. The overvoltage protection circuit consisting of two clamping diodes D_{c1} and D_{c2}, is not involved with the switching commutation process. It is only used to protect the auxiliary switches against voltage overshoot and oscillation caused by the resonance between the parasitic capacitance of auxiliary switches and the resonant inductor [21]. Three such single-phase ARCPIs with auxiliary branches

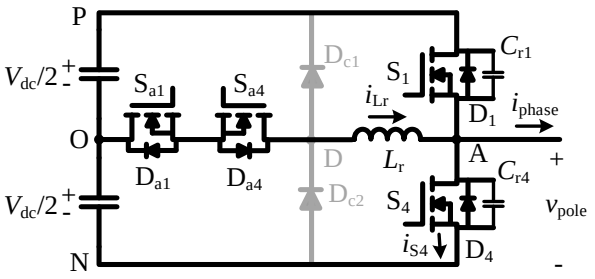

Fig. 1. The circuit schematic of the single-phase ARCPI [34].

connecting to the same DC middle point O can form a three-phase ARCPI. The positive polarities of voltage and current are shown as in Fig. 1.

B. Operation of the ARCPI

In the ARCPI, all the main switches perform ZVS and all the auxiliary switches perform ZCS during switching transitions, which reduces the switching loss and improves the inverter efficiency [22]. During a switching process, the resonant inductor L_r resonates with the two snubber capacitors C_{r1}, C_{r4} to create zero voltage across main switches. In this way, the main switches are turned on/off under ZVS and the output voltage waveform is smoothed in a sinusoidal way [23].

The detailed commutation processes of the ARCPI are illustrated in [21, 22, 34]. Only the turn-on process when the phase current i_{phase} >0, is described briefly in this section. Fig. 2 and Fig. 3 show the sub-circuits and the waveforms of gate signals, voltage and current of each stage during a turn-on process, respectively [34].

As seen, the commutation process starts at t_1 with the auxiliary switch S_{a1} turning on. Due to S_{a1} is in series with the

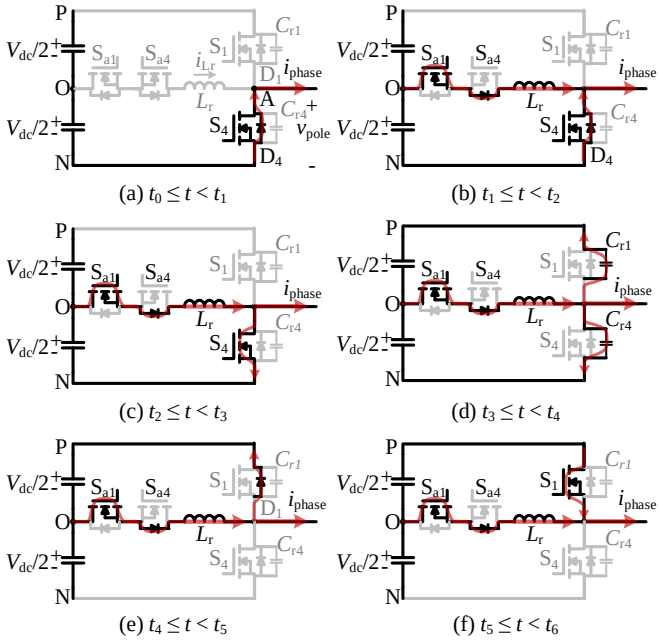

Fig. 2. The commutation process during main switch S_1 turn-on when $i_{phase} > 0$ [34].

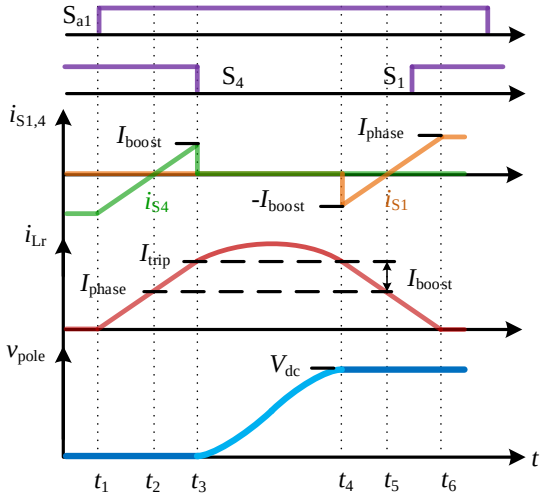

Fig. 3. Gate signals, main switches current, resonant inductor current, and output voltage during the turn-on process when $i_{phase} > 0$ [34].

resonant inductor L_r, the current flowing through the auxiliary branch increases from zero and the auxiliary switch S_{a1} performs ZCS turn-on. With the inductor current i_{Lr} ramping up, the main switch S_4 current i_{S4} starts to decrease at the same rate. At t_2, the inductor current i_{Lr} exceeds phase current I_{phase} and continues increasing, and i_{S4} reverses and then increases in the opposite direction.

When i_{Lr} reaches to its prescribed trip current I_{trip}, the switch S_4 is then turned off with the turn-off gate signal V_{g4} imposed on it. At this instant, the inductor L_r starts to resonate with the two snubber capacitors C_{r1} and C_{r4}.

The duration of the ramp up time t_{ramp} can be expressed as:

$$t_{ramp} = t_3 - t_1 = \frac{2L_r I_{trip}}{V_{dc}} \tag{1}$$

During the resonant interval t_{res}, the output voltage V_{pole} of the ARCPI increases in a sinusoidal profile until it is clamped to the dc bus voltage V_{dc} by the antiparallel diode D_1 of the main switch S_1 at t_4.

The resonant interval t_{res} can be given as follows [34]:

$$t_{res} = t_4 - t_3 = \frac{2}{\omega_r}\tan^{-1}\left(\frac{V_{dc}}{2Z_r(I_{trip} - I_{phase})}\right) \tag{2}$$

Where, ω_r and Z_r are the resonant frequency and resonant impedance of the ARCPI, respectively. ω_r and Z_r are given as in (3) and (4).

$$\omega_r = \sqrt{1/2L_rC_r} \tag{3}$$

$$Z_r = \sqrt{L_r/2C_r} \tag{4}$$

With the antiparallel diode D_1 conducting after t_4, the voltage across S_1 is clamped to zero. Then $-V_{dc}/2$ is applied to the resonant inductor L_r with i_{Lr} ramping towards zero and S_1 can be turned on. To ensure S_1 is turned under zero voltage condition, the turn-off signal must be imposed on S_1 before the

current though D_1 decreases to zero. Otherwise, the two capacitors will be charged and discharged by S_1 rather than the resonant inductor causing large overcurrent drawn through S_1, which will increase its losses and decrease the stability of the circuit [35].

After t_5, i_{Lr} decreases to I_{phase} and continues to ramp down to zero and the main switch S_4 current i_{S4} increases with the same rate. At t_6, i_{Lr} is zero and the auxiliary branch is disabled as the antiparallel diode D_{a4} in the auxiliary branch naturally turns off. After then, all the phase current flows through the main switch S_4. Then the gate signal of S_{a1} can be removed and the ARCPI reaches the steady state.

C. Experimental Setup

For the comparison, a 3-phase 6 kW ARCPI using Si IGBTs and a 3-phase 6 kW ARCPI using SiC MOSFETs are designed and built. Given the circuit parasitic parameters affect the converter performance, in order to get an objective result, the ARCPI using Si IGBTs or SiC MOSFETs are built on the same hardware platform shown as in Fig. 4.

The SiC MOSFETs are Wolfspeed C2M0040120D and the Si IGBTs are Infineon IKW40N120T2. These two switching devices have the same voltage/current rating (1200V/40A), and the same packaging (TO-247-3). Table I shows the main parameters of the switching devices [36, 37]. As seen, the minimum/maximum gate voltages of the SiC MOSFET and the Si IGBT are -10V/+25V and -20V/+20V, respectively. The gate driver with -5V/+15V gate signal can ensure these two switching devices switch properly since the gate threshold voltage are 2.6 V and 5.8 V for SiC MOSFETs and Si IGBTs, respectively. SiC MOSFETs with higher gate driver voltage can reduce the conduction resistance, however, the switching speed remains very similar because the switching speed is mainly determined by the gate resistance rather than the maximum gate driver voltage. Therefore, the same gate driver with -5V/+15V driving voltage has been used to carry out a like-for-like comparison and reveal the opportunities brough in by the fast switching speed of SiC MOSFETs. The driver is implemented with an ACPL-W484 optocoupler, a MGJ2D051500SC DC/DC converter, and an IXDN609SI driver. The selection of the gate resistance value is a balance between switching loss, voltage/current overshoots, ringings, EMI and cross-talk effects between the top and bottom devices, etc. A gate resistance of 25 Ω is used for both gate drivers.

The resonant circuit parameter selection is the heart of the design of the ARCPI. Its parameter can be designed for the purpose of either improving the system efficiency or attenuating the EMI [22]. The trade-off between loss and EMI performance need to be considered. With moving to fast-switching SiC MOSFETs, the EMI becomes a more severe issue. Since the ARCPI can significantly reduce the dv/dt by profiling the output voltage waveform, it is conceivable that the EMI noise generated by a hard-switching inverter could be attenuated by the ARCPI. Therefore, this paper applies the method presented in [22] with the purpose of improving the high frequency harmonic spectrum rather than purely reducing the switching loss. The parameters are shown in Table II.

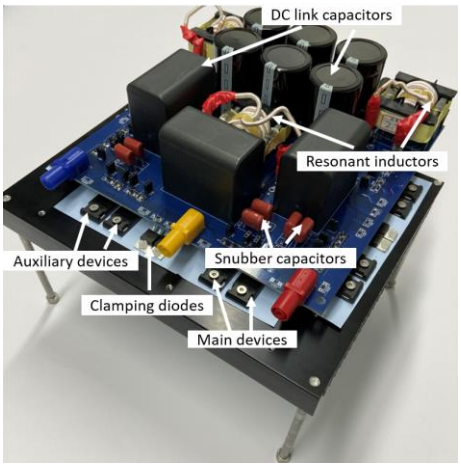

Fig. 4. Experimental prototype of the ARCPI.

TABLE I MAIN PARAMETERS OF THE SI IGBT AND SIC MOSFET

Parameter	SiC MOSFET	Si IGBT
Power device	C2M0040120D	IKW40N120T2
Voltage rating (V)	1200	1200
Current rating (A)	40	40
Minimum and maximum gate voltage (V)	+25/-10	+20/-20
Gate threshold voltage (V)	2.6	5.8
Internal gate resistance (Ω)	1.8	--
Turn-on delay time (ns)	15	33
Rise time (ns)	52	28
Turn-off delay (ns)	26	314
Fall time (ns)	34	64
Diode forward voltage	3.3	1.8
On resistance (mΩ)	40	--
Collector-emitter saturation voltage (V)	--	1.75

TABLE II. EXPERIMENTAL PROTOTYPE PARAMETERS

Symbol	Value	Symbol	Value
dc-bus voltage (V_{dc})	600V	Snubber capacitance (C_r)	47 nF
Resonant inductance (L_r)	2.7 μH	Load inductance (L_{load})	1.2 mH
AC resistance of the Resonant inductor (R_L)	5.12 mΩ	Load resistance (R_{load})	11 Ω

The ARCPIs can be controlled by two classical control methods: fixed-timing control [25] and variable-timing control [29]. The fixed-timing control method is to keep the inductor current i_{Lr} ramp interval t_{ramp} fixed during each switching cycle. It is easy to implement but the resonant current does not change with the load current which increases the current stress and power loss. In contrast, variable-timing control can address this issue by adjusting the inductor current i_{Lr} ramp interval t_{ramp} according to the load current. It therefore requires load current value to implement the control algorithm and has higher control complexity.

In this paper, the simple fixed-timing control algorithm with t_{ramp} = 400 ns is used as an example for comparing the performance with Si IGBTs and SiC MOSFETs. The fundamental frequency and the switching frequency are 50 Hz

and 20 kHz respectively. The control algorithm is implemented on a control platform based on a TI TMS320F28335 DSP and a Xilinx XC3S400 FPGA. The PWM signals are generated by the FPGA and the flowchart for the control method used in this paper is shown in Fig. 5. Noting that the time of t_{ramp}, t_{dead} and t_{aux} are set in the FPGA since it remains the same in every switching cycle.

Regarding the measurement, phase current, resonant inductor current, main switching device voltage/current and gate signals, and the output voltage of the ARCPI are measured using high-bandwidth voltage and current probes. To get these signals simultaneously, two oscilloscopes (MSO-X 3054A), working in master/slave mode, are used.

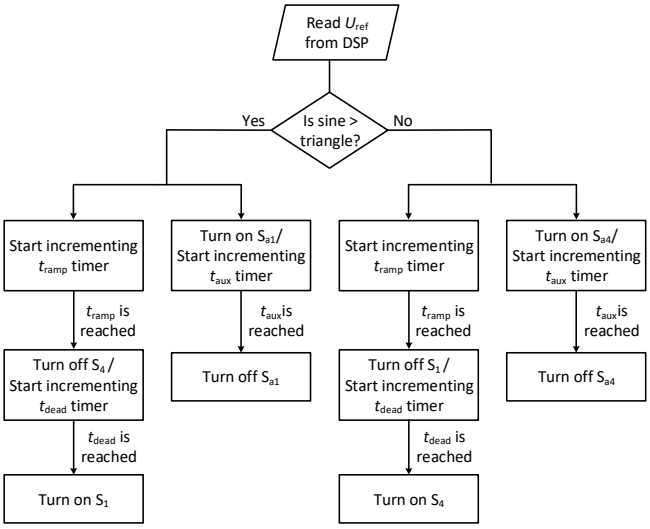

Fig. 5. Flowchart of the SPWM algorithm for the ARCPI.

III. Experimental Results and Analysis

For the performance comparison, only the results of Phase A are presented and analyzed in this paper as the results of the three-phase are symmetric.

A. Results over Fundamental Cycles

Fig. 6 shows the output voltage V_{pole}, the phase current i_A, the main switch S_4 current i_{S4}, and the resonant inductor current i_{Lr}, for two fundamental cycles using Si IGBTs in Fig. 6 (a) and SiC MOSFETs in Fig. 6 (b).

As seen, the phase currents are similar and the maximum phase current i_A of the ARCPI using Si IGBTs and SiC MOSFETs are 22.2 A and 22.1 A respectively. The output voltage V_{pole}, the main switch current i_{S4} and the inductor current i_{Lr} vary with the phase current i_A. However, compared with using Si IGBTs in Fig. 6 (a), the overshoot of V_{pole}, the main switch current i_{S4} and the inductor current i_{Lr} using SiC MOSFETs in Fig. 6 (b) are much smaller. The maximum V_{pole} is 541.5 V for Si IGBTs and 525.1 V for SiC MOSFETs. The maximum amplitude of i_{S4} and i_{Lr} is 99.6 A and 74.8A for Si IGBTs. In contrast, the maximum i_{S4} and i_{Lr} is 84.3 A and 70.8A for SiC MOSFETs. The RMS values of the main switch S_4 current i_{S4} are 9.7 A and 9.2 A using Si IGBTs and SiC MOSFETs, respectively. The RMS values of the inductor

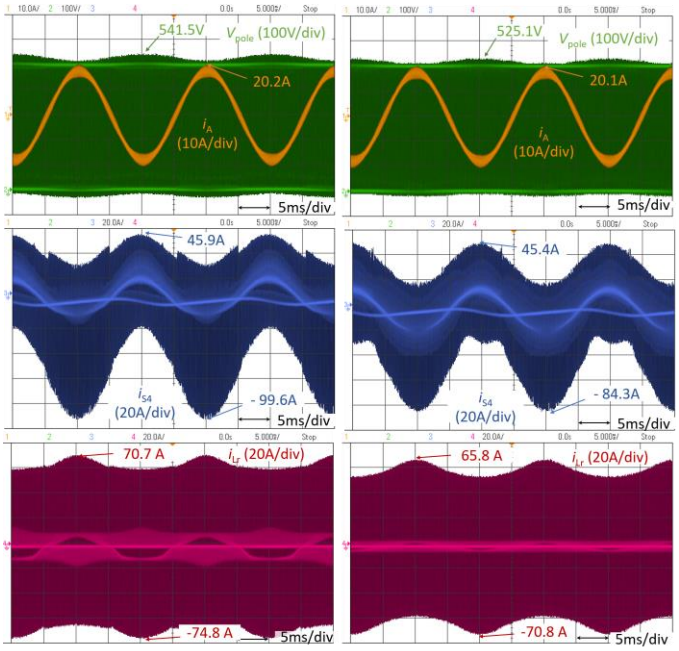

(a) (b)

Fig. 6. The output voltage V_{pole}, the phase current i_A, the main switch S_4 current i_{S4}, and the resonant inductor current i_{Lr}, for two fundamental cycles of the ARCPI using Si IGBTs in Fig. 6 (a) and SiC MOSFETs in Fig. 6 (b). V_{pole} 100 V/div, i_A 10 A/div, i_{Lr} 20 A/div, i_{S4} 20 A/div, time 5 ms/div.

current i_{Lr} are 13.2 A and 11.3 A using Si IGBTs and SiC MOSFETs, respectively.

Overall, the switching devices in the IGBT-based ARCPI endure higher voltage and current stress. This is caused by the turn-off delay of Si IGBTs which puts much more additional resonant energy into the circuit than what has been designed. The following part will analyze this aspect in detail.

According to (1), the resonant inductor trip current I_{trip} can be derived as:

$$I_{\mathrm{trip}} = \frac{V_{\mathrm{dc}} t_{\mathrm{ramp}}}{2L} \tag{5}$$

During the resonant interval, the maximum inductor current $I_{Lr\text{-}pk}$ can be given as follows [23]:

$$I_{\mathrm{Lr-pk}} = I_{\mathrm{phase}} + \sqrt{\left(\frac{V_{\mathrm{dc}}}{2Z_{\mathrm{r}}}\right)^2 + \left(I_{\mathrm{trip}} - I_{\mathrm{phase}}\right)^2} \tag{6}$$

When the turn-off delay t_d of the main switch S_4 is considered, the actual inductor trip current I'_{trip}, can be given by:

$$I'_{\mathrm{trip}} = \frac{V_{\mathrm{dc}}(t_{\mathrm{ramp}} + t_{\mathrm{d}})}{2L} \tag{7}$$

Submitting (7) into (6) gives the actual maximum inductor current:

$$I'_{\mathrm{Lr-pk}} = I_{\mathrm{phase}} + \sqrt{\left(\frac{V_{\mathrm{dc}}}{2Z_{\mathrm{r}}}\right)^2 + (I'_{trip} - I_{phase})^2} \tag{8}$$

According to (7) and (8), the actual current stress for the main switches and auxiliary switches are higher than the designed due to the turn-off delay of the main switch t_d.

Submitting (7) into (2) gives the actual resonant interval t'_{res}:

$$t'_{res} = \frac{2}{\omega_r}\tan^{-1}\left(\frac{V_{dc}}{2Z_r(I'_{trip} - I_{phase})}\right) \quad (9)$$

Comparing (2) and (9), it is clear that the actual resonant interval is shorter, and the output voltage waveform edge is steeper than the designed which will increase the high-frequency harmonics, thus deteriorating the EMI performance of the ARCPI.

Therefore, the actual waveforms during the turn-on commutation process can be depicted by the dash lines shown as in Fig. 7 [34]. As seen, when the turn-off gate signal V_{g4} is imposed on S_4 at t_3, S_4 is not turned off instantaneously because of the turn-off delay. S_4 is actually turned off at t'_3. Under this condition, i_{S4} keeps increasing until t'_3. Hence, the ramping up interval increases from t_{ramp} to t'_{ramp}, the inductor trip current increases from I_{trip} to I'_{trip} and the main switch current i_{S4} increases from I_{boost} to I'_{boost}. Therefore, more energy is put into the resonant circuit than the designed, the switches endure higher current stress and the output voltage waveform deviates from the designed shape and become steeper.

According to Table I, the typical turn-off delay for Si IGBTs and SiC MOSFETs is 314 ns and 26 ns, respectively. This means, using Si IGBTs in the ARCPI will increase current stresses and deteriorate the EMI performance due to the turn-off delay. In contrast, with little delay of SiC MOSFETs, the current stress is much smaller and the switching transition behaviour matches the ideal waveform.

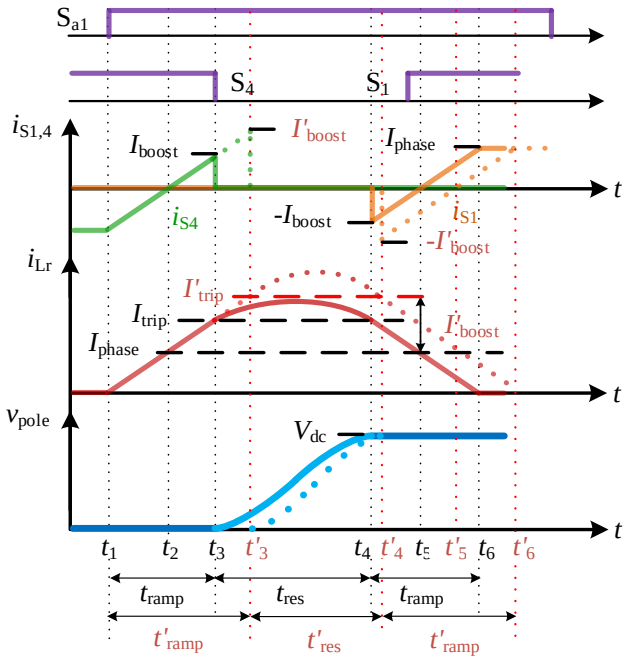

Fig. 7. Gate signals, main switches current, resonant inductor current, and output voltage during the turn-on process when the turn-off delay S_4 is considered [34].

B. Switching Transition Waveforms

In order to verify the above analysis, the switching transition waveforms of using Si IGBTs or SiC MOSFETs when $i_{phase} > 0$ are captured and analyzed in this section.

1) Turn-on process

Fig. 8 and Fig. 9 show the phase current i_A, the gate source signal V_{g1}, the source current i_{S1}, the drain source voltage V_{s1} for the main switch S_1, as well as the inductor current i_{Lr}, the gate source signal V_{g4}, the source current i_{S4}, the drain source voltage V_{S4} for the main switch S_4 using Si IGBTs or SiC MOSFETs, respectively during the turn-on transition when i_A is 9 A.

As seen in Fig. 8, the main switch S_1 performs ZVS turn-on as i_{S1} and V_{S1} are decoupled. The maximum current through S_1 and its the antiparallel diode are 33.7 A and -22.5A, respectively. The current i_{S4} ramps up with i_{Lr} and then changes its polarity at t_2. After that, a transient forward voltage drop of 17.9 V across the main switch S_4 is observed because the current is forced through the channel before the build-up of stored charge. This would lead to additional loss. At t_3, when the turn-off gate signal V_{g4} is imposed on S_4, the main switch S_4 is not turned off immediately, matching with the above theoretical analysis. The turn-off delay is about 311 ns. In this

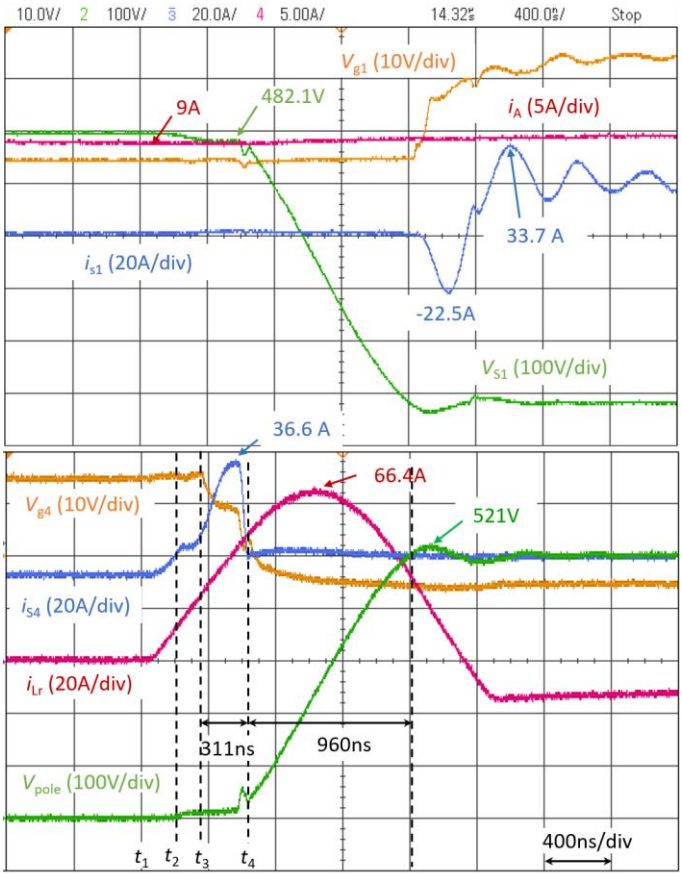

Fig.8. Phase current i_A, gate source signal V_{g1}, source current i_{S1} and drain source voltage V_{s1} for the main switch S_1, inductor current i_{Lr}, gate source signal V_{g4}, source current i_{S4} and drain source voltage V_{S4} for the main switch S_4 in the ARCPI using Si IGBTs during the turn-on transition when i_A = 10 A, i_A 10 A/div, V_{g1} 10 V/div, i_{S1} 20 A/div, V_{S1} 100 V/div, V_{g1} 10 V/div, i_{Lr} 20 A/div, i_{S4} 20 A/div, V_{pole} 100 V/div, time 400 ns/div.

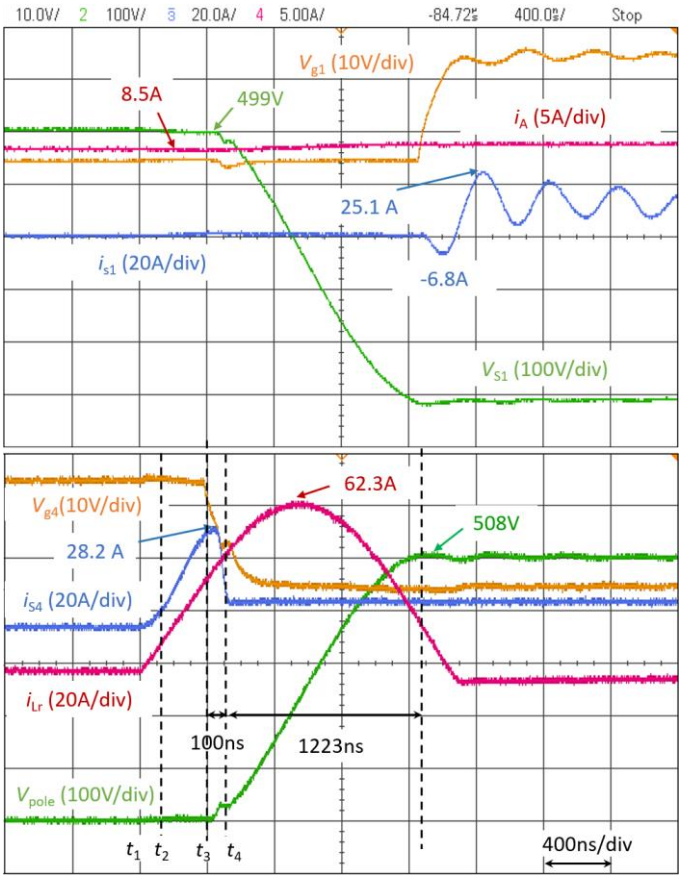

Fig.9. Phase current i_A, gate source signal V_{g1}, source current i_{S1} and drain source voltage V_{s1} for the main switch S_1, inductor current i_{Lr}, gate source signal V_{g4}, source current i_{S4} and drain source voltage V_{S4} for the main switch S_4 in the ARCPI using SiC MOSFETs during the turn-on transition when i_A = 10 A, i_A 10 A/div, V_{g1} 10 V/div, i_{S1} 20 A/div, V_{S1} 100 V/div, V_{g1} 10 V/div, i_{Lr} 20 A/div, i_{S4} 20 A/div, V_{pole} 100 V/div, time 400 ns/div.

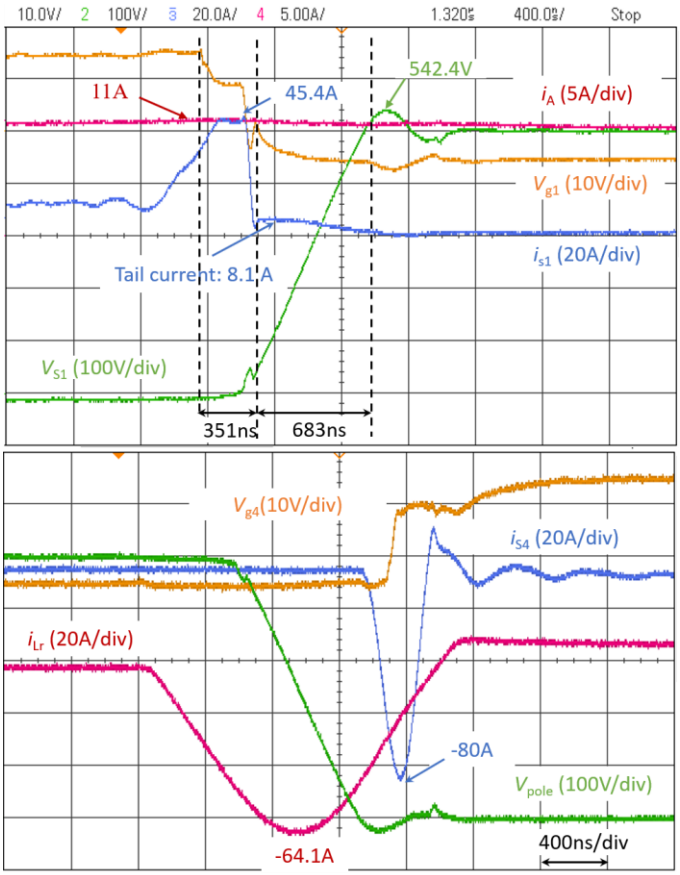

Fig.10. Phase current i_A, gate source signal V_{g1}, source current i_{S1} and drain source voltage V_{s1} for the main switch S_1, inductor current i_{Lr}, gate source signal V_{g4}, source current i_{S4} and drain source voltage V_{S4} for the main switch S_4 in the ARCPI using Si IGBTs during the turn-off transition when i_A = 11 A, i_A 10 A/div, V_{g1} 10 V/div, i_{S1} 20 A/div, V_{S1} 100 V/div, V_{g1} 10 V/div, i_{Lr} 20 A/div, i_{S4} 20 A/div, V_{pole} 100 V/div, time 400 ns/div.

case, the turn-off delay of S_4 forces its current i_{S4} to increase from 25 A to 46 A, and the trip current I_{trip} increases to 36.6 A. This means more energy is put into the resonant circuit resulting in a larger resonant current and faster resonant process than the designed. Under this condition, the peak resonant current is 66.4 A and the resonant interval is 960 ns.

For the SiC case, as seen in Fig. 9, the maximum current through S_1 and its antiparallel diode are much smaller, peaking at 25.1 A and -6.8 A, respectively. Similarly, i_{S4} peaks at 28.2 A instead of 46 A, and i_{Lr} peaks at 62.3A instead of 66.4 A. The major reason is that the energy put into resonance decreases due to the turn-off delay of SiC MOSFETs is much smaller. This way, the output voltage is smoother with a rise time of 1223 ns. The conduction loss in the auxiliary circuit will be reduced. Moreover, compared with Fig. 8, there is no significant forward voltage drop across the main switch during the ramping up period which could further reduce the loss.

2) Turn-off process

Fig. 10 and Fig. 11 show the experimental results during the turn-off transition when i_A = 11 A.

As seen, similar phenomena to the turn-on transition are observed. Compared with using Si IGBTs in Fig. 10, using SiC MOSFETs in Fig. 11 the turn-off delay decreases from 351 ns to 128 ns forcing less energy to put into the circuit. Overall, it is beneficial for reducing the current stress and attenuating the high-frequency harmonic, with the maximum inductor current decreasing from 64.1 A to 59.5 A, the maximum i_{S4} decreasing from 80 A to 66.7 A, the rise time of the output voltage increasing from 683 ns to 701 ns.

Besides the turn-off delay of the Si IGBT, the tail current of S_1 is also observed in Fig. 10. As seen, the main switch S_1 is not turned off completely because of the tail current when the output voltage V_{pole} starts increasing. Thus, using IGBTs does not perform ideal ZVS as the current and voltage are not fully decoupled. As a result, additional switching loss will be introduced. In contrast, as seen in Fig. 11 the current and voltage are decoupled fully, so the switching loss in the SiC MOSFETs will be removed.

C. The Current Stress and Resonant Interval

According to (2) and (6), the current stress of switching devices and the resonant interval during the switching transient are only affected by the load current and the trip current. The switching frequency and power factor have no effect on these two elements. In this paper, the trip current keeps the same as the fixed-timing control method is adopted. Therefore, the

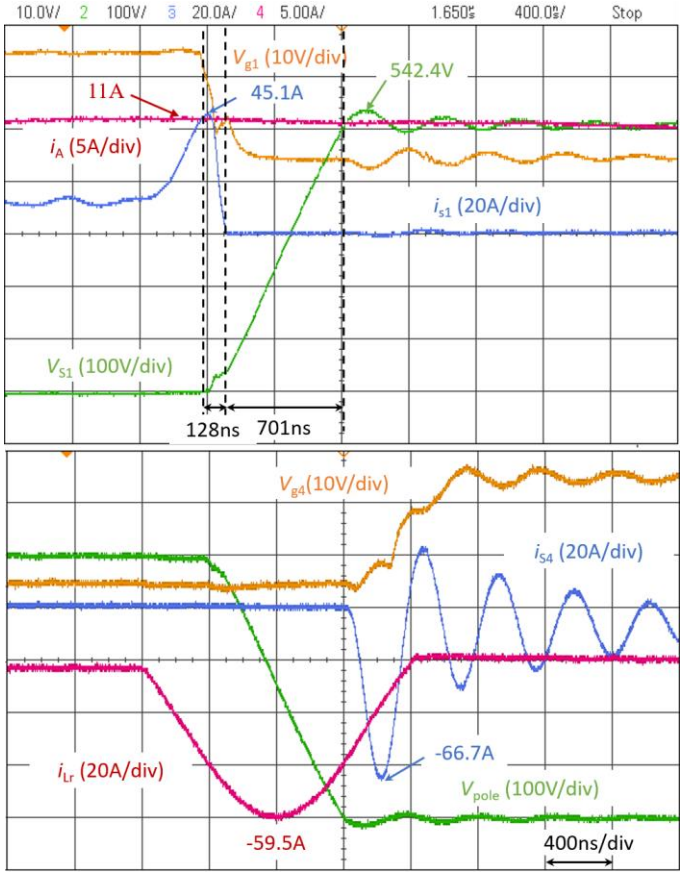

Fig. 11. Phase current i_A, gate source signal V_{g1}, source current i_{S1} and drain source voltage V_{s1} for the main switch S_1, inductor current i_{Lr}, gate source signal V_{g4}, source current i_{S4} and drain source voltage V_{S4} for the main switch S_4 in the ARCPI using SiC MOSFETs during the turn-off transition when i_A = 11 A, i_A 10 A/div, V_{g1} 10 V/div, i_{S1} 20 A/div, V_{S1} 100 V/div, V_{g1} 10 V/div, i_{Lr} 20 A/div, i_{S4} 20 A/div, V_{pole} 100 V/div, time 400 ns/div.

following parts compare the current stress and resonant interval using Si IGBTs or using SiC MOSFETs at different load current conditions.

With experimental results, Fig. 12 and Fig.13 compare the maximum current of the main switch S_4 i_{S4}, and the maximum resonant inductor current i_{Lr} using Si IGBT or SiC MOSFETs at various phase current levels. Fig. 14 compares the resonant interval with Si IGBTs or SiC MOSFETs.

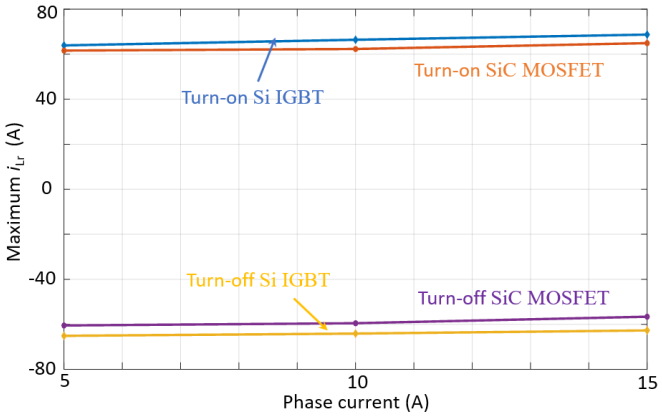

Fig. 12. The maximum resonant inductor current for the ARCPI using Si IGBTs or SiC MOSFETs during switching transitions at different load current.

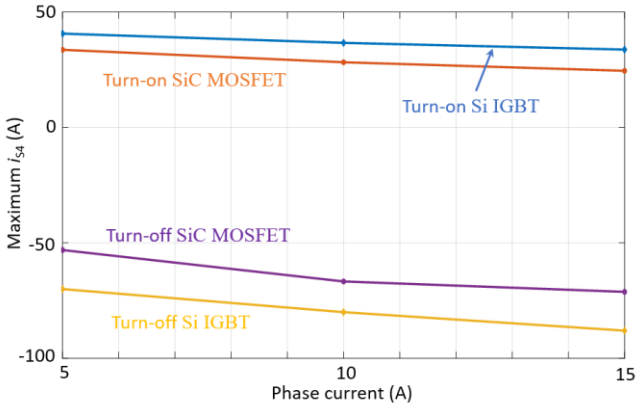

Fig. 13. The maximum main switching current i_{S4} for the ARCPI using Si IGBTs or SiC MOSFETs during switching transition at different load current.

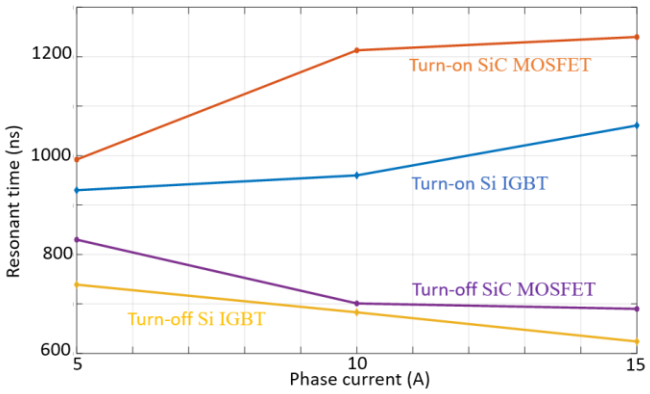

Fig. 14. The resonant interval t_{res} for the ARCPI using Si IGBTs or SiC MOSFETs during switching transitions at different load current.

As seen in Fig. 12 and Fig.13, the maximum inductor current i_{Lr} and main switching current i_{S4} using SiC MOSFETs are smaller than using Si IGBTs. Hence, the switches in the SiC ARCPI endure less current stress at different load conditions. As seen in Fig. 14, the resonant interval with SiC MOSFETs is much longer than that of the Si IGBTs. Thus, using SiC MOSFETs has smoother output waveform resulting in an attenuated high-frequency response.

D. Ripple Current in the Capacitor Bank

In the three-phase ARCPI, the ripple current i_{CO} in the bottom dc-link capacitor is shaped by the simultaneous currents in all the three auxiliary branches due to the auxiliary branches connecting to the same neutral point O. The ripple current in the dc-link capacitors can be given by

$$i_{CO} = \frac{(i_{LrA} + i_{LrB} + i_{LrB})}{2} \qquad (10)$$

Where, i_{LrA}, i_{LrB} and i_{LrC} are the resonant current in phase A, B, C, respectively.

Fig. 15 shows the simulation results of the three resonant inductor currents and the bottom dc-link capacitor current i_{CO}. As seen, the maximum current ripple is determined by the maximum resonant inductor current. Fig. 16 compares the

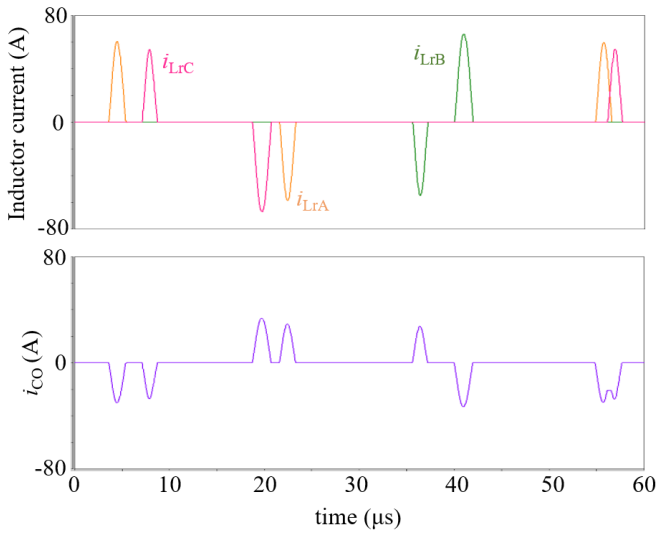

Fig. 15. The current in auxiliary branches A, B, and C i_{LrA}, i_{LrB} and i_{LrC}, and the bottom dc-link capacitor i_{CO}.

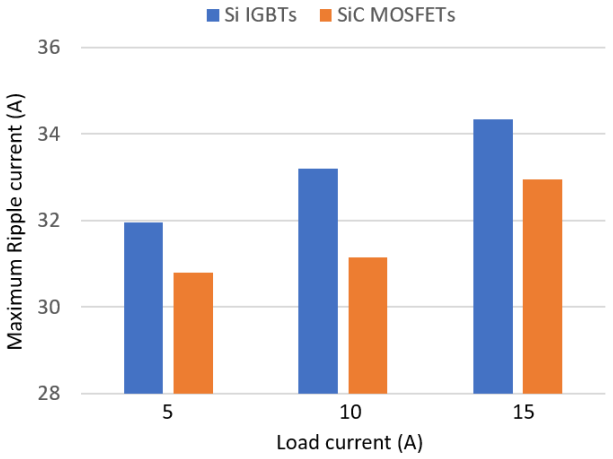

Fig. 16. The maximum ripple current in the dc-link capacitor for the ARCPI using Si IGBTs or SiC MOSFETs during switching transitions at different load current.

maximum ripple current thought the bottom dc-link capacitor at different load conditions. As seen, the maximum ripple current for SiC MOSFETs is 3.5% less than that for Si IGBTs.

E. EMI Performance

Fig. 17 shows the output voltage frequency spectrum of the ARCPI using Si IGBTs or SiC MOSFETs. As seen, below 550 kHz, the ARCPI using Si IGBTs and SiC MOSFETs have similar harmonics. However, with SiC MOSFETs, the harmonics is lower above 550 kHz. Specifically, a maximum 20 dBμV harmonic reduction can be achieved at 800 kHz. This is because the output voltage edge of the ARCPI using SiC MOSFETs is smoother than that of using Si IGBTs as analyzed in above section.

F. The Total Loss and Efficiency

The total loss and efficiency of using Si IGBTs or SiC MOSFETs are measured. Experimental results show that when

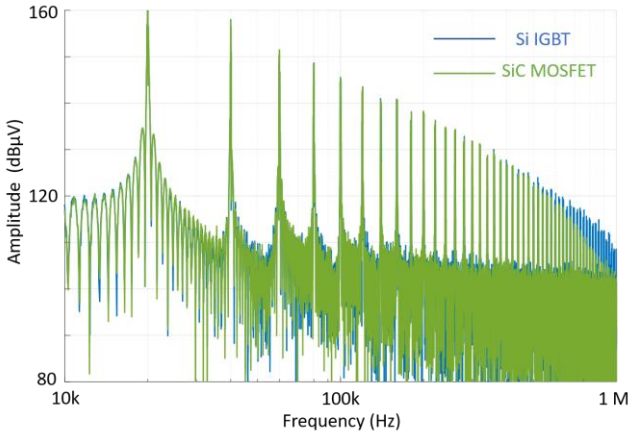

Fig. 17. Output voltage frequency response of the ARCPI using Si IGBTs or SiC MOSFETs.

the output power is 6 kW, the total loss of the ARCPI using SiC MOSFETs and IGBTs is 289 W and 501 W, respectively. Therefore, when the output power is 6 kW, the efficiency of using SiC MOSFETs and IGBTs is 95.4% and 92.3% respectively. It means the efficiency of the ARCPI using SiC MOSFETs is 3.1% higher than that of Si IGBTs. The loss and efficiency quoted here includes all the losses in the circuit including the main and auxiliary switching devices, resonant inductors and capacitors, filters, busbar, etc. The lower efficiency with Si IGBTs is because the turn-off delay and the tail current of the main switches. As analyzed above, the turn-off delay of the main switch causes much more current flowing though switching devices and the resonant inductor, resulting in higher conduction losses. The incomplete decoupling between current and voltage results in higher switching loss.

It is worth noting that the SiC MOSFETs and Si IGBTs are driven by the same gate drivers with -5V/+15V driving voltage, 25 Ω gate resistance. In this case, SiC MOSFETs are not being used at its maximum potential. Compared with the gate driver with the recommended driving voltage of -5V/+20V, the gate driver used in this experiment increases the on-state resistance ($R_{ds(ON)}$) of SiC MOSFETs by about 30% at 25°C [37], hence higher conduction losses. Also, using a smaller gate drive resistance e.g. 2.5 Ω can significantly increase the switching speed and reduce the resonant current in the auxiliary resonant circuit. Therefore, the efficiency of the SiC MOSFET ARCPI can be further improved when using a -5V/+20V driving voltage and 2.5Ω gate resistance.

G. The Size of Passive Components

The resonant circuit parameters (resonant inductor and capacitor values) can be designed for the purpose of either improving the system efficiency or attenuating the EMI. This paper designs the ARCPI with the purpose of improving the EMI performance rather than purely reducing the power loss. The resonant interval t_{res} and trip current I_{trip} are set the same for Si IGBTs and SiC MOSFETs.

According to (2)(3)(4), the resonant inductance (L_r) and capacitance (C_r) are only determined by the resonant interval and trip current. Therefore, the passive components such as

resonant inductors and capacitors for SiC MOSFETs and Si IGBTs should be the same. However, due to the SiC converter has a higher efficiency, the cooling requirement such as heatsink or fan can be smaller.

H. Component Cost

Fig. 18 compares the normalized cost of the two prototypes. The cost includes the power switching devices, PCBs, gate drivers, dc-link capacitors, resonant inductors, resonant capacitators, heatsinks and auxiliary components. The cost of each component of the converter is the average price from commercial suppliers. As seen, the cost of the ARCPI using SiC MOSFETs is about 80% higher than that using Si IGBTs. The major reason is that the cost of SiC MOSFETs is much higher than that of Si IGBTs. However, with the increased adoption of SiC devices and mass production, the cost of SiC MOSFETs will go down in future.

It is worth noting that while the cost of the SiC prototype is higher than that of Si IGBT prototype, the efficiency of SiC MOSFETs is 3.1% higher than Si IGBTs at full load condition. Therefore, the heatsink of the ARCPI using SiC MOSFETs can be smaller, and the total cost of SiC ARCPI can be further reduced.

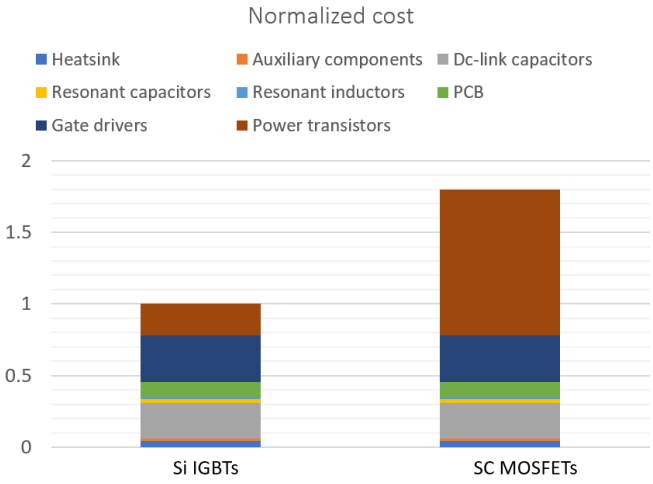

Fig. 18. The normalized cost of the ARCPI using Si IGBTs or SiC MOSFETs.

IV. Conclusion

The performance of the ARCPI using Si IGBTs or SiC MOSFETs has been evaluated comprehensively in experiment. It has shown that the ARCPI using MOSFETs has better performance than that using Si IGBTs because of the shorter turn-off delay of SiC MOSFETs. Firstly, the ARCPI using SiC MOSFETs performs full ZVS and the switching transition behaviour is more predictable. Unlike Si IGBTs, SiC MOSFETs have shorter turn-off delay, no turn-off tail current and no forward voltage drop during switching transitions. Thus, there is almost no switching loss in the SiC MOSFETs. Secondly, the switches in the ARCPI using SiC MOSFETs endures less current stress and less ripple current in the neutral point when compared to that of Si IGBTs. In the ARCPI, the main switch turn-off delay introduces additional energy into the resonant circuit, resulting in higher current stress on switches, steeper output voltage edge and more conduction loss. Due to the fast turn-off speed of SiC MOSFETs, the current stress caused by the turn-off delay is smaller than that of the Si IGBTs counterpart. Thirdly, the ARCPI using SiC MOSFETs exhibits better EMI performance and higher efficiency. Specifically, a maximum 20 dBμV harmonic content reduction can be achieved at 800 kHz and a 3.1% efficiency improvement can be achieved at 6 kW with SiC MOSFETs than those with Si IGBTs. However, the cost of the ARCPI using SiC MOSFETs is about 80% higher than that using Si IGBTs.

Acknowledgment

The authors would like to thank the technical input from Dr. Ian Laird at the University of Bristol on the converter hardware design.

References

[1] X. Yuan, "Application of Silicon Carbide (SiC) Power Devices: Opportunities, Challenges and Potential Solutions," *in IECON 2017 - 43rd Annual Conference of the IEEE Industrial Electronics Society*, Beijing, China, 2017, pp. 893–900.

[2] X. She, A. Q. Huang, Ó. Lucía and B. Ozpineci, "Review of Silicon Carbide Power Devices and Their Applications," *IEEE Transactions on Industrial Electronics*, vol. 64, no. 10, pp. 8193-8205, Oct. 2017.

[3] A. Marzoughi, R. Burgos and D. Boroyevich, "Characterization and Performance Evaluation of the State-of-the-Art 3.3 kV 30 A Full-SiC MOSFETs," *IEEE Transactions on Industry Applications*, vol. 55, no. 1, pp. 575-583, Jan.-Feb. 2019.

[4] G. Rizzoli, M. Mengoni, L. Zarri, A. Tani, G. Serra and D. Casadei, "Comparative Experimental Evaluation of Zero-Voltage-Switching Si Inverters and Hard-Switching Si and SiC Inverters," *IEEE Journal of Emerging and Selected Topics in Power Electronics*, vol. 7, no. 1, pp. 515-527, March 2019.

[5] C. D. Fuentes, S. Kouro and S. Bernet, "Comparison of 1700-V SiC-MOSFET and Si-IGBT Modules under Identical Test Setup Conditions," *IEEE Transactions on Industry Applications*, vol. 55, no. 6, pp. 7765-7775, Nov.-Dec. 2019.

[6] X. She, P. Losee, H. Hu, W. Earls and R. Datta, "Performance Evaluation of 1.5 kV Solar Inverter With 2.5 kV Silicon Carbide MOSFET," *IEEE Transactions on Industry Applications*, vol. 55, no. 6, pp. 7726-7735, Nov.-Dec. 2019.

[7] Z. Zeng and X. Li, "Comparative Study on Multiple Degrees of Freedom of Gate Drivers for Transient Behavior Regulation of SiC MOSFET," *IEEE Transactions on Power Electronics*, vol. 33, no. 10, pp. 8754-8763, Oct. 2018.

[8] L. Zhang, X. Yuan, X. Wu, C. Shi, J. Zhang and Y. Zhang, "Performance Evaluation of High-Power SiC MOSFET Modules in Comparison to Si IGBT Modules," *IEEE Transactions on Power Electronics*, vol. 34, no. 2, pp. 1181-1196, Feb. 2019.

[9] Q. Yan, X. Yuan, Y. Geng, A. Charalambous and X. Wu, "Performance Evaluation of Split Output Converters with SiC MOSFETs and SiC Schottky Diodes," *IEEE Transactions on Power Electronics*, vol. 32, no. 1, pp. 406-422, Jan. 2017.

[10] I. Laird, X. Yuan, J. Scoltock and A. J. Forsyth, "A Design Optimization Tool for Maximizing the Power Density of 3-Phase DC–AC Converters Using Silicon Carbide (SiC) Devices," *IEEE Transactions on Power Electronics*, vol. 33, no. 4, pp. 2913-2932, April 2018.

[11] A. Schroedermeier and D. C. Ludois, "Integration of Inductors, Capacitors, and Damping into Bus Bars for Silicon Carbide Inverter dv/dt Filters," *IEEE Transactions on Industry Applications*, vol. 55, no. 5, pp. 5045-5054, Sept.-Oct. 2019.

[12] J. Kim, D. Shin and S. Sul, "A Damping Scheme for Switching Ringing of Full SiC MOSFET by Air Core PCB Circuit," *IEEE Transactions on Power Electronics*, vol. 33, no. 6, pp. 4605-4615, June 2018.

[13] F. Qi, M. Wang and L. Xu, "Investigation and Review of Challenges in a High-Temperature 30-kVA Three-Phase Inverter Using SiC MOSFETs," *IEEE Transactions on Industry Applications*, vol. 54, no. 3, pp. 2483-2491, May-June 2018.

[14] I. Laird and X. Yuan, "Analysing the Crosstalk Effect of SiC MOSFETs in Half-Bridge Arrangements," in *2019 IEEE Energy Conversion Congress and Exposition (ECCE)*, Baltimore, MD, USA, 2019, pp. 367-374.
[15] P. Wang, L. Zhang, X. Lu, H. Sun, W. Wang and D. Xu, "An Improved Active Crosstalk Suppression Method for High-Speed SiC MOSFETs," *IEEE Transactions on Industry Applications*, vol. 55, no. 6, pp. 7736-7744, Nov.-Dec. 2019.
[16] P. Nayak and K. Hatua, "Parasitic Inductance and Capacitance-Assisted Active Gate Driving Technique to Minimize Switching Loss of SiC MOSFET," *IEEE Transactions on Industrial Electronics*, vol. 64, no. 10, pp. 8288-8298, Oct. 2017.
[17] N. Oswald, P. Anthony, N. McNeill, and B. H. Stark, "An Experimental Investigation of the Tradeoff between Switching Losses and EMI Generation with Hard-switched All-Si, Si-SiC, and All-SiC Device Combinations," *IEEE Transactions on Power Electronics*, vol. 29, no. 5, pp.2393–2407, May 2014.
[18] S. Walder and X. Yuan, "Effect of Load Parasitics on the Losses and Ringing in High Switching Speed SiC MOSFET based Power Converters," in *2015 IEEE Energy Conversion Congress and Exposition (ECCE)*, Montreal, QC, Canada, 2015, pp. 6161-6168.
[19] S. Walder, X. Yuan, I. Laird and J. J. O. Dalton, "Identification of the Temporal Source of Frequency Domain Characteristics of SiC MOSFET based Power Converter Waveforms," in *2016 IEEE Energy Conversion Congress and Exposition (ECCE)*, Milwaukee, WI, USA, 2016, pp. 1-8.
[20] X. Yuan, C. Wei, W. Zhou and G. Wang, "A Novel Five-Level Converter for Medium-Voltage Power Conversion Systems," in *IECON 2019 - 45th Annual Conference of the IEEE Industrial Electronics Society*, Lisbon, Portugal, 2019, pp. 4953-4958.
[21] W. Zhou, X. Yuan, and I. Laird, "Elimination of Overshoot and Oscillation in the Auxiliary Branch of a SiC Auxiliary Resonant Commutated Pole Inverter (ARCPI)" in *ICPE 2019 – ECCE Asia, 10th International Conference on Power Electronics*, Busan, Korea (South), 2019, pp. 383-389.
[22] A. Charalambous, X. Yuan, and N. McNeill, "High-Frequency EMI Attenuation at Source with the Auxiliary Commutated Pole Inverter," *IEEE Transactions on Power Electronics*, vol. 22, no. 7, pp. 5660-5676, July 2018.
[23] V. Pickert and C. M. Johnson, "Three-phase Soft-switching Voltage Source Converters for Motor Drives. I. Overview and Analysis," in *IEE Proceedings - Electric Power Applications*, vol. 146, no. 2, pp. 147-154, March 1999.
[24] D. M. Divan and G. Skibinski, "Zero-switching-loss Inverters for High-power Applications," *IEEE Transactions on Industry Applications*, vol. 25, no. 4, pp. 634-643, July-Aug. 1989.
[25] R. W. De Doncker and J. P. Lyons, "The Auxiliary Resonant Commutated Pole Converter," *in IEEE Industry Application Society Annual Meeting*, Seattle, WA, USA, 1990, vol. 2, pp. 1228-1235.
[26] O. D. Patterson and D. M. Divan, "Pseudo-resonant Full Bridge dc/dc Converter," *IEEE Transactions on Power Electronics*, vol. 6, no. 4, pp. 671-678, Oct. 1991.
[27] Y. C. Jung, H. L. Liu, G. C. Cho, and G. H. Cho, "Soft Switching Space Vector PWM Inverter using a New Quasi-parallel Resonant dc Link," *in 26th IEEE Power Electronics Specialists Conference*, Atlanta, GA, USA, 1995, pp. 936-942, vol.2.
[28] J. G. Cho, H. S. Kim, and G. H. Cho, "Novel Soft Switching PWM Converter using a New Parallel Resonant dc-link," *in 22nd IEEE Power Electronics Specialists Conference*, Cambridge, MA, USA, 1991, pp. 241-247.
[29] C. C. Chan, K. T. Chau, D. T. W. Chan, J. Yao, J. S. Lai and Y. Li, "Switching Characteristics and Efficiency Improvement with Auxiliary Resonant Snubber based Soft-switching Inverters," *in 29th Annual IEEE Power Electronics Specialists Conference*, Fukuoka, Japan, 1998, pp. 429-435, vol.1.
[30] J. S. Lai, J. Zhang, H. Yu, and H. Kouns, "Source and Load Adaptive Design for a High-power Soft-switching Inverter," *IEEE Transactions on Power Electronics*, vol. 21, no. 6, pp. 1667-1675, Nov. 2006.
[31] D. Rothmund, D. Bortis and J. W. Kolar, "Accurate Transient Calorimetric Measurement of Soft-Switching Losses of 10-kV SiC MOSFETs and Diodes," *IEEE Transactions on Power Electronics*, vol. 33, no. 6, pp. 5240-5250, June 2018.
[32] R. Li, Z. Ma, and D. Xu, "A ZVS Grid-connected Three-phase Inverter," *IEEE Transactions on Power Electronics*, vol. 27, no. 8, pp. 3595-3604, Aug. 2012.
[33] M. Yamamoto, "Full SiC Soft Switching Inverter — Stability Performance for False Turn on Phenomenon," in *2013 IEEE 10th* International *Conference on Power Electronics and Drive Systems (PEDS)*, Kitakyushu, Japan, 2013, pp. 159-164.
[34] W. Zhou, X. Yuan, and I. Laird, "Performance Comparison of the Auxiliary Resonant Commutated Pole Inverter (ARCPI) using SiC MOSFETs or Si IGBTs" in *2019 IEEE Energy Conversion Congress and Exposition (ECCE)*, Baltimore, MD, USA, 2019, pp. 1981-1987.
[35] K. Ma, D. Xu, T. Zhang and S. Igarashi, "The Evaluation of Control Strategies for Auxiliary Resonant Commutated Pole Inverter," in *2009 IEEE Energy Conversion Congress and Exposition*, San Jose, CA, USA, 2009, pp. 810-816.
[36] IKW40N120T2 [online] https://www.infineon.com/dgdl/Infineon-IKW40N120T2-DS-v02_04-EN.pdf?fileId=db3a304412b407950112b42%206d87b3ad5.
[37] C2M0040120D [online] https://www.wolfspeed.com/media/downloads/165/C2M0040120D.pdf.

Wenzhi Zhou (S'18) received the B.S. degree from Dalian Jiaotong University, Dalian, China, and the M.Sc. degree from Zhejiang University, Hangzhou, China, in 2013 and 2016, respectively, both in electrical engineering. He is current working toward the Ph.D. degree with the Electrical Energy Management Group, Department of Electrical and Electronic Engineering, University of Bristol, Bristol, U.K.

His research interests include wide-bandgap device applications, soft-switching, partial discharge and motor drives.

Xibo Yuan (S'09-M'11-SM'15) received the B.S. degree from China University of Mining and Technology, Xuzhou, China, and the Ph.D. degree from Tsinghua University, Beijing, China, in 2005 and 2010, respectively, both in electrical engineering.

He has been a Professor since 2017 in the Electrical Energy Management Group, Department of Electrical and Electronic Engineering, University of Bristol, Bristol, U.K, where he became Lecturer, Senior Lecturer and Reader in 2011, 2015 and 2016, respectively. He also holds the Royal Academy of Engineering/Safran Chair in Advanced Aircraft Power Generation Systems. He is an executive committee member of the UK National Centre for Power Electronics and the IET Power Electronics, Machines and Drives (PEMD) network.

His research interests include power electronics and motor drives, wind power generation, multilevel converters, application of wide-bandgap devices, electric vehicles and more electric aircraft technologies. Professor Yuan is an Associate Editor of IEEE Transactions on Industry Applications and IEEE Journal of Emerging and Selected Topics in Power Electronics. He is a Fellow of IET and received The Isao Takahashi Power Electronics Award in 2018.